The Embrace Magnetometer Network for South America: Network Description and Its Qualification

C. M. Denardini[1], S. S. Chen[1], L. C. A. Resende[1], J. Moro[2,3], A. V. Bilibio[1], P. R. Fagundes[4], M. A. Gende[5], M. A. Cabrera[6,7], M. J. A. Bolzan[8], A. L. Padilha[1], N. J. Schuch[2], J. L. Hormaechea[5,9], L. R. Alves[1], P. F. Barbosa Neto[1,10], P. A. B. Nogueira[11], G. A. S. Picanço[1], and T. O. Bertollotto[1,12]

[1]National Institute for Space Research (INPE), São José dos Campos, São Paulo, Brazil, [2]Southern Regional Space Research Center in collaboration with the LACESM/CT-UFSM, Santa Maria, Rio Grande do Sul, Brazil, [3]State Key Laboratory of Space Weather, National Space Science Center, Chinese Academy of Science (CAS), Beijing, China, [4]IP&D, Universidade do Vale do Paraíba, São José dos Campos, São Paulo, Brazil, [5]Facultad de Ciencias Astronómicas y Geofísicas, Universidad Nacional de La Plata (UNLP) and CONICET, La Plata, Buenos Aires, Argentina, [6]Laboratorio de Telecomunicaciones, Departamento de Electricidad, Electrónica y Computación, Facultad de Ciencias Exactas y Tecnología (FACET), Universidad Nacional de Tucumán (UNT), San Miguel de Tucumán, Tucumán, Argentina, [7]Centro de Investigación sobre Atmósfera Superior y Radiopropagación, Facultad Regional Tucumán, Universidad Tecnológica Nacional (UTN), San Miguel de Tucumán, Tucumán, Argentina, [8]Departamento de Física, Universidade Federal de Jataí (UFG), Jataí, Goiás, Brazil, [9]Estación Astronómica Rio Grande (EARG), Facultad de Ciencias Astronómicas y Geofísicas (FCAG), Universidad Nacional de La Plata (UNLP), Rio Grande, Terre del Fuego, Argentina, [10]Departamento de Engenharia Elétrica, Centro Universitário Salesiano de São Paulo (Unisal—Campus São Joaquim), Lorena, São Paulo, Brazil, [11]Federal Institute of Education, Science and Technology of São Paulo, Jacareí, São Paulo, Brazil, [12]Departamento de Engenharia Elétrica, Universidade de Taubaté (UNITAU), Taubaté, São Paulo, Brazil

Abstract The present work is the first of a two-part paper on the Embrace Magnetometer Network. In this part, we present the new Embrace Magnetometer Network (Embrace MagNet) in South America, which is originally planned to cover most of the eastern portion of the Southern America longitudinal sector by installing and operating fluxgate magnetometer stations. We discuss the purpose and scientific goals of the network, associated with aeronomy and space weather. We provide details on the instrumentation, location of the sensors, sensitivity matching process, gain matching process, and magnetometer installation. In addition, we present and discuss details about the data storage, near-real time display, and availability.

Plain Language Summary This manuscript introduces the reader to the new Embrace Magnetometer Network (Embrace MagNet), which is located in South America and is based on fluxgate magnetometer. Its main purpose is to fulfill the gap in magnetic measurements, which are suitable for space weather purpose. Details on the instrumentation, location of the sensors, sensitivity matching process, gain matching process, and magnetometer installation are provided in this first of a two-part paper on the Embrace MagNet. The accompanying paper provides information on the first scientific findings.

1. Introduction

No comprehensive studies on global ionospheric current sheets (Chapman & Bartels, 1940; Lindzen & Chapman, 1969; Maeda & Kato, 1966; Matsushita, 1969; Vestine, 1960) were carried out in the South American sector. Most of the magnetic data currently available have been collected in several sectors, but in the eastern South American sector, which has a completely different magnetic configuration at the low latitudes, ranging from 0° in its western portion to −20° of magnetic declination at some points of the eastern edge. Only recently few studies have been carried out, for example, on geomagnetically induced currents in the grounded conducting networks (Trivedi et al., 2007) and on the counterelectrojet (Denardini et al., 2009). In addition, there is growing concern about the space weather effects (see definition in Denardini et al., 2016a) to the current technological assets (Schrijver et al., 2015), which may lead to estimated global economic impact ranging from $2.4 to $3.4 trillion USD over 1 year if a Quebec-like 1989 event occurred nowadays (Schulte in den Bäumen et al., 2014).

Accordingly, the Brazilian Study and Monitoring of Space Weather (Embrace) Program developed the Embrace Magnetometer Network (Embrace MagNet) to cover most of the eastern South American longitudinal sector
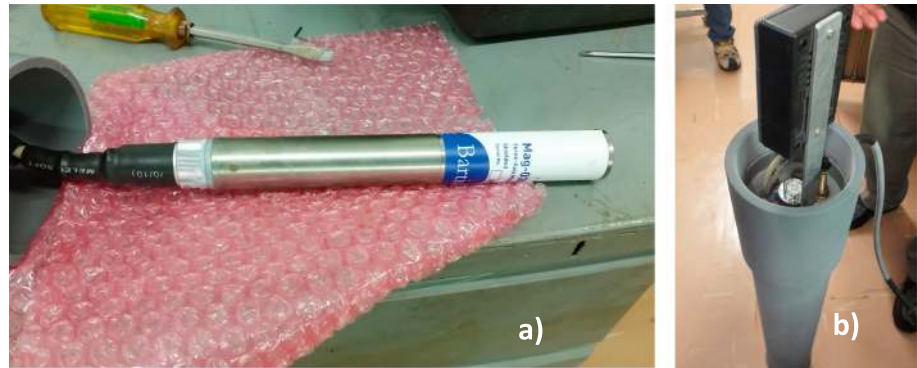
Figure 1. Picture of (a) the single bar sensor core that is built inside (b) the sealed magnetometer sensors PVC enclosure, which composes the Embrace MagNet magnetometer system.

(Denardini et al., 2016b). This network fills the gap of magnetic measurements available online in this sector and aims to provide magnetic data to be used as an estimate of the regional disturbance level (Denardini et al., 2015) caused by the geomagnetic storms (Gonzalez et al., 1994) driven by the space weather effects, for example, by developing the South American K (Ksa) index. Besides, a long-term scientific goal is to investigate the trends in the magnetic intensity of the South America Magnetic Anomaly and the implication of its presence in the deviation of the magnetic indices used to monitor the solar-terrestrial relationship associated with space weather, in a framework similar to that proposed by Moro et al. (2012).

Under this context, it should be noticed that we are currently developing a network that covers continental dimensions. On one hand, by installing a magnetometer network in a range of approximately 50° × 40° (latitude and longitude) in the South American sector, we expect to acquire enough data to help the scientific community to explore whether responses to magnetic storms in the eastern or in the western South American sector are different or similar. On the other hand, maintaining such a network requires a lot of effort, including long journeys to carry out repairs or maintenances. Thus, a cooperative pull of institutions with engaged personnel is essential.

In the present paper, as the first of a two-part paper on the Embrace Magnetometer Network, we provide details on the instrumentation used in the Embrace MagNet, on the sensitivity matching process for the sensors, on the gain matching process for the Embrace MagNet in comparison to the Intermagnet data, on the Embrace MagNet data quality check.

2. Magnetometer Descriptions and Specifications

The Embrace Program chose a three-axis fluxgate magnetometer manufactured by the Jicamarca Radio Observatory (e.g., type number is JRO-ML-103) to compose the Embrace MagNet. This type of magnetometer is sensitive to the magnetic field in the range up to 1 mT with achievable resolution down to 10 pT, through measuring direct current (DC) or low-frequency alternating current (AC) magnetic fields. The principle of the fluxgate is based on the excitation current through the excitation coil producing field that periodically saturates the soft magnetic material of the sensor core (usually made of FeCoNi, FeNi, MoFeNi, and CoFeSiCr alloy), and the magnetic field measurement is made by using the voltage induced in the coil direction (Ripka, 1992). Voltage changes are proportional to the measured variation in the horizontal (H), declination (D), or vertical (Z) components of the geomagnetic field.

The Embrace MagNet magnetometer sensors is an old version of the Mag-03 Three-Axis Magnetic Field Sensors manufactured by Bartington that use single bars with a high level of magnetic saturation, covered with two copper coils, one for the excitation and the second for sensing the external field (Figure 1a). It was built for compact and high

Table 1
Basic Characteristics of the Fluxgate Magnetometers of the Embrace MagNet

Description	Range/values
Total measurement range	±75,000 nT
Dynamic range, three selectable	±250, 1,000, and 2,500 nT
Maximum resolution	0.1 nT
Accuracy	0.25%
Orthogonality	<0.5°
Offset at 25℃, 1 atm	<1 nT
Zero drift	<0.1 nT/℃
Operating temperature	−20℃ to +75℃

```
CACHOEIRA PAULISTA EMBRACE-01 <001> 1 Sec. Raw data

HH MM SS   H(Ch2)    D(Ch4)    Z(Ch6)    T1(Ch7) T2(Ch8)

12 00 00  -0077668 -0036585 -0101692 0056192 0049044
12 00 01  -0077673 -0036590 -0101680 0056189 0049042
12 00 02  -0077682 -0036597 -0101674 0056189 0049039
12 00 03  -0077701 -0036588 -0101683 0056191 0049039
12 00 04  -0077709 -0036589 -0101682 0056190 0049038
12 00 05  -0077711 -0036599 -0101674 0056188 0049036
```

Figure 2. A sample of a primary output ASCII file provided by the fluxgate magnetometer.

performance precision measurements of the Earth's magnetic field vector, operating at any location where the magnetic field lies on the ±75,000 nT range. However, the acquisition software only allows three acquisition ranges: ±250 nT, ±1,000 nT, or ±2,500 nT. These ranges are enough to cover the amplitude of the diurnal variations of the magnetic components from low to high latitude (Veliz, 2010). The system can be powered by either any 220/110 VAC or ±12 VDC power supply, and the outputs are in the form of three analog voltages from 0 to ±2.5 VDC, proportional to the three geomagnetic vector components. The compact fluxgate sensor is assembled in a cylindrical weatherproof double wall PVC enclosure (Figure 1b). It is 104 cm long and has a diameter of 18 cm. It ensures high mechanical and thermal stability. A front-end low noise amplifier is installed overhead the sealed sensor core along with a circular bubble level. The former is responsible for introducing gain in the measurements in order to ensure that the sensor will be installed tens of meters apart from the control system and the power supply. The latter is used for precise leveling of the sensor during the installation procedure.

The electronic control unit encompasses all the other parts need to acquire, digitally convert the voltage into long integer numbers, monitor, and transfer the information to the accompanying computer. The data acquisition module rate is 20 bits and is set together with the electronic control unit and the USB data output. Data acquisition and monitoring software include both local data storage and simultaneous upload to two different data archive servers, assuring real-time data availability. The data time stamp can be controlled either by the computer associated to the system or by the GPS receiver attached to the external antenna. In case of using the computer associated to the system, the clock is corrected by international time servers provided through the Internet (e.g., time.nist.gov) every hour. The main magnetometer characteristics specified by the manufacturers are summarized in Table 1.

The primary output files provided are ASCII files within the 1 s time resolution raw measurement (the long integer numbers) of the horizontal (H), declination (D), and vertical (Z) magnetic vector components besides the temperature at controller room (T_1) and the buried sensor (T_2), as shown in Figure 2. Such files contain 1 h of data only, and the location where the magnetometer is stalled is printed on the header of every file together with system ID (Embrace-01 in this example), the computer operating system characterization, the time resolution, and the file type.

While acquiring data, the monitoring software also appends the 1 min averaged values of above quantities to the preprocessed daily ASCII file. These 1 min averaged values are obtained by averaging the 60 values of the

```
CACHOEIRA PAULISTA EMBRACE-01 <001> 1 Min. Reported data

DD MM YYYY  HH MM   H(mV)     D(mV)     Z(mV)    T1(mV)  T2(mV)

01 01 2012  11 58  -370.632 -175.169 -485.234 268.211 234.657
01 01 2012  11 59  -369.495 -174.181 -485.080 268.214 234.310
01 01 2012  12 00  -370.691 -174.090 -485.000 268.215 233.914
01 01 2012  12 01  -369.456 -172.235 -485.184 268.215 233.775
01 01 2012  12 02  -370.278 -172.265 -485.076 268.213 234.103
```

Figure 3. A sample of a preprocessed daily ASCII file provided by monitoring software.

```
CACHOEIRA PAULISTA EMBRACE-01 <001> 1 Min. Reported data

DD MM YYYY  HH MM   D(Deg)   H(nT)    Z(nT)     I(Deg)    F(nT)


01 01 2012  11 58  -21.5242 17347.2 -13768.4 -38.4389 22147.2
01 01 2012  11 59  -21.5229 17347.7 -13768.4 -38.4380 22147.5
01 01 2012  12 00  -21.5228 17347.2 -13768.4 -38.4387 22147.1
01 01 2012  12 01  -21.5204 17347.7 -13768.4 -38.4381 22147.5
01 01 2012  12 02  -21.5204 17347.4 -13768.4 -38.4385 22147.2
```

Figure 4. A sample of a final daily ASCII file provided by monitoring software.

corresponding variables acquired during the corresponding minute, that is, from the second 0.000 to the second 59.999. During this process, these long integer numbers are converted to voltage levels, as shown in Figure 3. The head of the file keeps the same information mentioned above.

Finally, the data are converted back in their original units, and the magnetic dip angle (I) and the module of the main field (F) are also calculated and added to the final ASCII file. The temperatures are dropped out from this final file since they are used for eventual data correction only. A sample of a final daily ASCII file provided by the monitoring software is shown in Figure 4.

3. Basic Description of Embrace Magnetometer Network

3.1. Location of the Embrace MagNet Stations

The Embrace MagNet is planned to cover most of the eastern portion of the Southern America longitudinal sector in order to fulfill a gap for magnetic measurement available online. The availability of fast Internet, reliable energy supply, and easy access was the key points for deciding the exact location of the magnetometer

Table 2
Geographical Location of the Embrace MagNet Stations (and Candidate Stations) With the Corresponding Magnetic Latitude, Designed Code, Dip Angle, and Date When the Operation Started (or That Is Planned to Start)

Geomag. lat. (°)	Location (city and state/province)	Code	UN[a]	Geographic		Altitude (m)	Dip (°)	Operational since/*planned*
				Latitude	Longitude			
+09.4	Boa Vista, RR	BOA	BR	02°48′02″N	60°40′33″W	076	+18.80	*12/2019*
+04.4	Manaus, AM	MAN	BR	02°53′18″S	59°58′11″W	102	+08.09	06/2016
	Porto Velho, RO	PVE	BR	08°45′49″S	63°54′23″W	083		*12/2019*
−00.4	Belém, PA	BLM	BR	01°26′28″S	48°26′40″W	016	−00.80	*12/2020*
−03.6	São Luís, MA	SLZ	BR	02°35′39″S	44°12′35″W	032	−07.26	12/2011
−03.7	Alta Floresta, MT	ALF	BR	09°52′13″S	56°06′15″W	284	−07.50	06/2014
−05.6	Araguatins, TO	ARA	BR	05°36′01″S	48°06′02″W	103	−11.30	09/2016
−08.2	Eusébio, CE	EUS	BR	03°52′48″S	38°25′28″W	043	−16.51	11/2011
−08.3	Palmas, TO	PAL	BR	10°17′50″S	48°21′41″W	231	−16.52	*12/2018*
−08.5	Cuiabá, MT	CBA	BR	15°33′17″S	56°04′10″W	233	−17.10	07/2014
	São João do Cariri, PB	CRR	BR	07°23′21″S	36°32′21″W	458		*12/2019*
−12.3	Jataí, GO	JAT	BR	17°55′55″S	51°43′05″W	679	−24.60	11/2013
−13.7	Campo Grande, MS	CGR	BR	20°30′24″S	54°37′04″W	540	−25.50	*12/2020*
−15.8	Tucumán, TU	TCM	AR	26°49′20″S	65°11′40″W	431	−27.35	10/2016
	Medianeira, PR	MED	BR	25°17′43″S	54°05′38″W	402		*12/2018*
−18.9	Cachoeira Paulista, SP	CXP	BR	22°42′07″S	45°00′52″W	601	−36.43	05/2011
−19.1	São José dos Campos, SP	SJC	BR	23°12′31″S	45°57′49″W	583	−36.64	05/2013
−19.7	Vassouras, RJ	VSS	BR	22°24′07″S	43°39′08″W	443	−38.40	05/2015
−21.6	São Martinho da Serra, RS	SMS	BR	29°26′37″S	53°49′22″W	462	−36.65	06/2013
	Chillán, CO	CHI	CH	36°38′15″S	71°59′57″W	124		*12/2018*
	Aiguá, MA	AIG	UY	34°12′16″S	54°45′38″W	112		*12/2020*
	Bahia Blanca, BA	BBA	AR	38°41′00″S	62°15′37″W	020		*12/2021*
−39.9	Rio Grande, TF	RGA	AR	53°47′09″S	67°45′42″W	010	−50.03	11/2012
−58.4	Estação Cmte. Ferraz, AC	ECF	BR	62°05′06″S	58°24′12″W	010	−53.20	*12/2021*

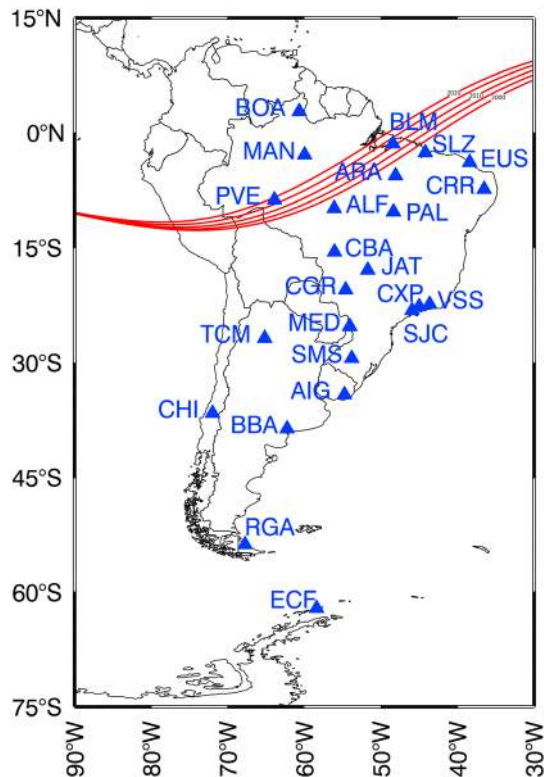[a]UN = Country, AR = Argentine, BR = Brazil, CH = Chile, UY = Uruguay.

Figure 5. Geographic distribution of the Embrace MagNet stations (and candidate stations) over South America.

stations of the Embrace MagNet. Table 2 presents the location of the Embrace MagNet stations, which started to be set in May 2011 and is originally planned to be concluded in December 2021.

The South America map with the geographic distribution of the Embrace MagNet stations (and candidate stations) is presented in Figure 5. The red lines in this figure show the location of the dip equator from 2000 to 2020 calculated with the International Geomagnetic Reference Field Model within 5 year steps. The time evolution of the dip equator is from the east to the west due to the secular variation of the Earth's main magnetic field, which is seen as a (mostly) westward displacement.

Each magnetic station is composed by the three-axis fluxgate magnetometer described above, a controller system and a personal computer for local data storage, and Internet FTP server. The sensor is buried 1 m deep, under a cover made of metal-free material to provide protection against moderate rain, winds, and solar exposure. This shelter is installed in a location 40 to 50 m apart from the main housing where the controller system and the personal computer are located. The cable that connects the magnetic sensor to the controller system is sealed, and it is buried 20 cm deep to avoid solar exposure, providing some temperature protection. The plugs of the connecting cable are military certified connectors to assure low noise connections, water resistance, and long durability. The room of the main housing is maintained under temperature control. Figure 6 shows some pictures of the sensor under the cover (picture a) and the system controller with the personal computer aside (picture b).

3.2. Sensitivity Matching Process of the Embrace MagNet Sensors

In order to assure the consistency of the magnetic measurements performed within the magnetometer that are part of this network, we calibrate each individual sensor against a reference fluxgate magnetometer. We adopted such approach for the sensitivity matching process of the whole network because the goals of the Embrace MagNet, which are associated with measuring the amplitude variation of the magnetic field in the entire South America, but not to obtain the absolute values instead. We assumed that one reference fluxgate magnetometer to the network would be enough for such process. Thus, we have chosen the magnetometer installed at CXP as the reference one. Thereafter, we take a mandatory procedure to submit all the magnetic equipment acquired to be part of the Embrace MagNet for a sensitivity matching process against the reference magnetometer. This procedure consists of the following:

1. Burying the sensor of the new magnetometer close (2–3 m) apart to the sensor of the reference fluxgate magnetometer, applying no changes to the factory settings;

Figure 6. Picture of (a) the magnetic sensor buried 1 m deep under a wood shelter and (b) the system controller with the personal computer for local data storage, and Internet FTP server at the SMS station.
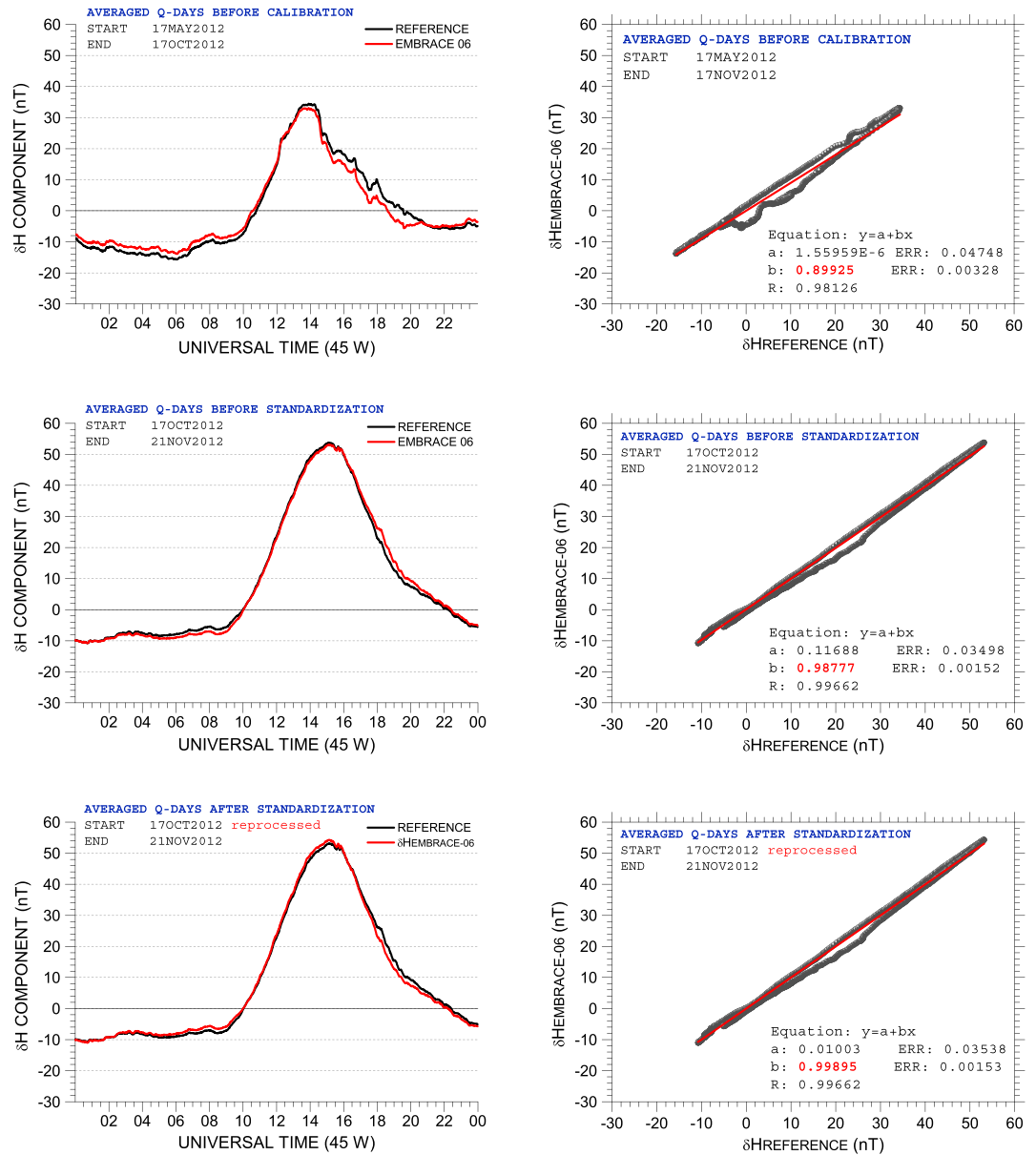
Figure 7. Example of a diurnal variation of the (left side) QDC under evaluation and reference QDC with the corresponding (right side) linear fit (upper panel) for the period of the calibration process, (middle panel) for the period of the standardization process, and (bottom panel) resulting from the sensitivity matching process.

2. Collecting data for three consecutive months with both equipment;
3. Selecting the data collected during the five most magnetic quietest days of each month with paying attention that the three-hourly Kp value never exceeds a value of 3 over the entire day;
4. Averaging the data acquired during the selected 5 days to obtain the mean quiet day curve (QDC; the QDC should be representative for the period of acquisition, avoiding aliasing, outliers, and any other possible interference) as described by Denardini et al. (2015) for each geomagnetic component (i.e., H, D, and Z) of each magnetometer individually;
5. Performing a correlation analysis between the three QDC (H, D, and Z) of the reference magnetometer and the three corresponding QDC of the magnetometer under evaluation;
6. Correcting the gain of the measurements of each individual magnetic component of the magnetometer under evaluation, based on the angular parameter derived from the estimated regression equation;

Table 3
List of the Maximum Perceptual Error of Each Magnetometer With Respect to the Reference Magnetometer

Magnetometer labels		Maximum error with respect to the reference							
		H		D		Z		F	
Reference	Under evaluation	$b-1$ (%)	a (nT)	$b-1$ (%)	a (°)	$b-1$ (%)	a (nT)	$b-1$ (%)	a (nT)
EMBRACE-01	EMBRACE-02	−0.059	−0.000	−0.053	−0.000	+0.112	+0.001	±0.037	±0.001
EMBRACE-01	EMBRACE-04	−0.246	+0.003	−0.199	+0.000	+0.648	+0.008	±0.286	±0.008
EMBRACE-05	EMBRACE-01	+0.103	+0.000	−0.157	+0.000	+0.079	−0.001	±0.129	±0.001
EMBRACE-05	EMBRACE-06	−0.105	+0.010	−0.015	−0.002	−0.073	−0.011	±0.126	±0.015
EMBRACE-05	EMBRACE-07	−0.028	+0.000	−0.068	+0.001	−0.083	+0.001	±0.078	±0.001
EMBRACE-05	EMBRACE-08	+0.178	−0.001	−0.121	+0.001	−0.103	+0.001	±0.053	±0.001
EMBRACE-05	EMBRACE-09	−0.099	+0.000	+0.089	+0.001	+0.041	+0.001	±0.041	±0.001
EMBRACE-05	EMBRACE-10	+0.149	−0.000	+0.092	+0.000	−0.003	0.000	±0.103	±0.000
EMBRACE-05	EMBRACE-11	+0.080	−0.000	+0.204	−0.000	+0.111	−0.000	±0.135	±0.000
EMBRACE-05	EMBRACE-12	+0.088	+0.000	−0.067	+0.000	+0.109	+0.338	±0.139	±0.256
EMBRACE-05	EMBRACE-13	+0.120	−0.000	−0.142	−0.000	+0.130	+0.000	±0.177	±0.000
EMBRACE-05	EMBRACE-14	−0.023	+0.000	+0.057	−0.000	−0.109	+0.000	±0.093	±0.000
EMBRACE-05	EMBRACE-15	+0.096	−0.000	−0.007	−0.000	+0.113	−0.000	±0.148	±0.000
EMBRACE-05	EMBRACE-16	+0.178	+0.000	+0.149	−0.000	+0.011	+0.000	±0.134	±0.000
EMBRACE-05	UNIVAP-01	−0.863	+0.015	+0.453	−0.000	+0.133	−0.068	±0.186	±0.059
EMBRACE-05	UNIVAP-02	−0.121	+0.000	−0.165	+0.000	−0.141	+0.000	±0.125	±0.000
EMBRACE-05	UNIVAP-03	−0.075	+0.000	−0.002	+0.000	−0.102	−0.000	±0.222	±0.000
Averaged square error		±0.154	±0.002	±0.120	±0.000	±0.124	±0.025	±0.130	±0.020

7. Collecting data for one more month; and
8. Repeating steps 3 to 6 to ensure an angular parameter derived from the estimated regression equation lies between 0.98 and 1.02 (i.e., a relative error lower than 2%).

Examples of the graphs obtained during the sensitivity matching process of each individual component of the magnetometer are shown in Figure 7. In the present case, we show the diurnal variation of the QDCs derived from the H component of the Earth's magnetic field acquired at CXP in the left graphs of this figure. The QDCs obtained for the period from 17 May to 16 October are shown in the upper panel and represent the data before calibration. The QDCs obtained for the period from 17 October to 21 November 2012 are shown in the middle panel and represent the data after calibration. The bottom panel brings the same graph as the middle panel but with the reprocessed data, after applying the correction from the sensitivity matching process. The red line identifies the QDC derived from the H component for the magnetometer under evaluation (named QDC under evaluation for simplification) while the black lines show the time evolution of the QDC derived from the H component for the reference magnetometer (named reference QDC for simplification).

The graphs on the right side of each panel of Figure 7 show the scatterplots (black dots) of the reference QDC versus the QDC under evaluation superimposed by the resulting linear fit (red line). Each linear fit graph on the right side corresponds to the analysis of the QDCs in the graph in the same row on the left side. The equation estimated from the regression and its parameters are included in the bottom right corner of these scatterplots. We highlight in red the angular coefficient that provides a direct view of the sensitivity matching between the two sensors.

In summary, the upper panel of Figure 7 illustrates the development of the procedure described above from 1 to 5 The middle panels of this figure illustrate the items 6 to 7 of the procedure. The lower panel illustrates the ending result of the sensitivity matching process. The maximum perceptual error ($b - 1$) between reference QDC versus the QDC under evaluation obtained after the sensitivity matching process for each magnetic component is presented in Table 3. In addition, the corresponding offset values (a) are present. In the bottom line of this table, we present the averaged square error and offset for each individual magnetic component. Lastly, we have calculated the averaged square error and offset for the total field, which are also presented in the last columns of Table 3. Considering a typical daily excursion of about ±200 nT for the horizontal component of the magnetic field under the magnetic equator (which is quite reasonable from our

Table 4

Specification and Operational Parameters of the Embrace MagNet and the Intermagnet for the Gain Matching Process

	Embrace MagNet	Intermagnet
Maximum resolution	0.1 nT	0.1 nT
Band pass	DC to 3 kHz	DC to 0.1 Hz
Sampling rate	1 Hz	1 Hz
Thermal stability	<0.1 nT/°C	0.25 nT/°C
Long term stability	Not available	5 nT/year

experience), the maximum error expected is about 0.308 nT. This error is of the order of the equipment maximum resolution (see Table 1).

3.3. Gain Matching Process for the Embrace MagNet

Following the sensitivity matching process, we subsequently proceeded to the gain matching procedure in order to assure that each sensor of the Embrace MagNet will provide amplitude values comparable to an IAGA standard magnetometer (Jankowski & Sucksdorff, 1996). The procedure used for matching the gain of the whole Embrace MagNet to absolute magnetic measurement by the Intermagnet Network was made at the VSS observatory (fluxgate for variations and proton precession magnetometers for absolute measurements). It consisted of two stages: (a) a frequency domain analysis and (b) a time domain analysis. The frequency domain analysis consists of an analysis of a linear regression to the frequency spectra of the magnetic data simultaneously collected by both magnetometers after using a high-pass filter (period superior to ~3 h). The time domain analysis consists of obtaining the Pearson product moment correlation between the individual magnetic components measured by the fluxgate and the proton precession magnetometer.

For the present process, we collected the horizontal (H), the declination (D), and the vertical (Z) components of the geomagnetic field from June 2015 until May 2016. The Embrace three-axis fluxgate magnetometer operated at the VSS observatory along with the proton precession magnetometer that was installed a few meters apart, which is part of the Intermagnet Network. The main specifications and operational parameters of both magnetometers that compose the Embrace MagNet and the Intermagnet are summarized in Table 4.

Therefore, the first stage of gain matching procedure was performed to evaluate the electromagnetic contamination of the magnetic measurements using spectral analysis. During the process, we have applied a low-pass filter to the data in order to select the portion of the spectrum with frequencies up to 0.1 mHz (periods superior than 2.77 h). The procedure applied to every single day of measurement was individually performed to both magnetometers (Embrace and Intermagnet) installed in VSS and comprises the following:

1. Apply a FFT to the 1 day data collected by each magnetometer at 1 min time resolution rate;
2. Select the portion of each daily power spectra comprising the frequencies up to 0.1 mHz (i.e., apply a low-pass filter to each spectrum);
3. Apply linear regression to each daily power spectra (i.e., $y = a + bx$, where y is the amplitude of the power spectrum and x is the power density per Hz); and
4. Calculate the daily averaged error between the linear regression and the power spectra.

In order to exemplify the results of this first stage, we present Figure 8. It shows the temporal evolution of the angular coefficient of the linear regression applied to each daily power spectra obtained from the data collected daily. The angular coefficients corresponding to the Embrace MagNet magnetometer are shown by the blue line with triangles, while same coefficients corresponding to the Intermagnet magnetometer are shown by red line with squares. The error bars correspond to the monthly averaged error between the linear regression and the power spectra of each individual analysis.

After compiling the results along the year of analysis as a temporal evolution of the angular coefficient of the linear regression, we are confident to state that the curves practically overlap. The values of each angular coefficient lie on the daily averaged error of each other curve, except for very few cases during maintenance of the equipment. This means that the data collected by an Embrace MagNet sensor is equivalent to the data provided by the Intermagnet Network in terms of the slope of the daily power spectra filtered to a period superior to ~3 h.
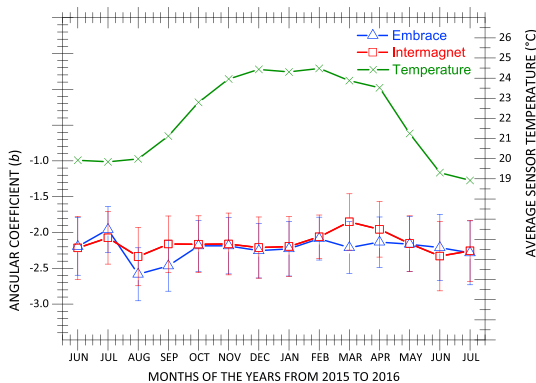

Figure 8. Temporal evolution of the (left side scale) angular coefficient of the linear regression applied to the daily power spectra obtained from the 1 day data collected at 1 min time resolution rate at the Magnetic Observatory of Vassouras from June 2015 to July 2016 by the Embrace MagNet magnetometer (blue line with triangles) and by the Intermagnet magnetometer (red line with squares). The monthly averaged temperature of the buried sensor is superimposed as the green line with "X" symbols and is referred to the right-side scale.

Table 5
Estimated Error (ε) of the Magnetic Components (H, D, Z) of Embrace MagNet on Quiet (Qday) and Disturbed (Dday) Days

Condition	ε_H	ε_D	ε_Z
Qday	0.04158	−0.16803	−0.05840
Dday	0.04161	−0.15319	−0.05776
Mean	0.04159	−0.16061	−0.05808
Percentage	4.2%	−16.1%	−5.8%

The monthly averaged temperature curve of the buried sensor is superimposed to the previous curves. It is identified as the green line with "X" symbols and is referred to the right-side scale. It shows that the averaged ground temperature rose from about 20°C in the winter of 2015 to roughly 24°C in the summer and went down to 19°C in the winter of 2016 (Southern Hemisphere). Thus, we can say that the overlap of the angular coefficients occurs irrespective of the temperature of the sensor.

In order to assure that, we have performed a straightforward analysis of equipment response to thermal variability. We calculated the ratio between the range (the difference between the maximum and the minimum of the curve) of the angular coefficients obtained from the linear regression applied to the daily power spectra and the maximum temperature range (the difference between the maximum and minimum curves) throughout the period of analysis. This analysis was made to the Embrace MagNet sensor and to the Intermagnet sensor. It resulted in 0.05 per Celsius for the Embrace MagNet and 0.06 per Celsius for the Intermagnet. Hence, the variations of the angular coefficients with the temperature are similar for both equipment, and the difference between these rates is very small, less than 0.98% in relative values.

The second stage of gain matching procedure was performed using the very raw data given in nT or degree (without applying any gain to the Embrace MagNet data). This second step consisted of comparing vis-a-vis the measurements during the five magnetically quietest days and the five most disturbed days covering the period of evaluation. Mathematically, the comparison consisted of performing a correlation analysis in the time domain. The basic procedure for this second step is as follows (considering the disturbance level):

1. Select the magnetic data covering the five quietest (five most disturbed) days in each month;
2. Subtract each magnetic data acquired during the five quietest (five most disturbed) days by its corresponding local midnight value (the derivation of the quietest (disturbed) daily ΔH is provided through the equation $\Delta H (t) = H(t) - H(00h00 \text{ LT})$, in which $H(t)$ is the daily variation of the horizontal component and "t" is the time (from 00h00 to 23h59 UT with 1 min resolution); the same formulation is individually applied to each component of the Earth's magnetic field);
3. Calculate the Pearson product moment correlation (r^2) between the ΔH, ΔD, and ΔZ components measured by the fluxgate and the proton precession magnetometer during the five quietest (five most disturbed) days of each month; and
4. Calculate the error (ε) between the Embrace MagNet and Intermagnet using the angular coefficient from the moment correlation of the quietest (most disturbed) period, which is the difference in electronic gains between the two magnetic sensors (the error (ε) between the Embrace MagNet and Intermagnet is calculated using the angular coefficient for each component of the Earth's magnetic field as $\varepsilon_{H,D,Z} = 1 - B_{H,D,Z}$, where "$B$" is the angular coefficient of the linear fit for each magnetic component (H, D, Z)).

The daily averaged correlation factors between the magnetic data collected by the Embrace MagNet and Intermagnet are presented and discussed in terms of the individual magnetic components, the magnetic activity, and the season of the year. In this context, J months encompass May, June, July, and August, and it represents the winter season for the southern hemisphere. The E months, enclosing March, April, September, and October, represent the equinox. Finally, D months correspond to November, December, January, and February and represent the southern hemisphere summer season.

The overall results of this second stage of gain matching procedure are shown in Table 5. The higher error is found in the D component (ε_D). The amplitude of the magnetometer under evaluation was around 16.1% higher than the reference magnetometer. The error in H component (ε_H) was around 0.042, which means the Embrace data had an amplitude of 4.2% lower than the Intermagnet data. The error in the Z component (ε_Z) had a gain of 5.8% in relation to the absolute magnetometer.

In general, the values of ε are satisfactory when considering the quiet and disturbed periods separately. We notice that there is a very small difference in the errors. This means that there is no appreciable difference when analyzing data collected during quiet or disturbed period. Thus, we may conclude that the correlation applies to any magnetic conditions. Moreover, we measured variations of the components of the Earth's
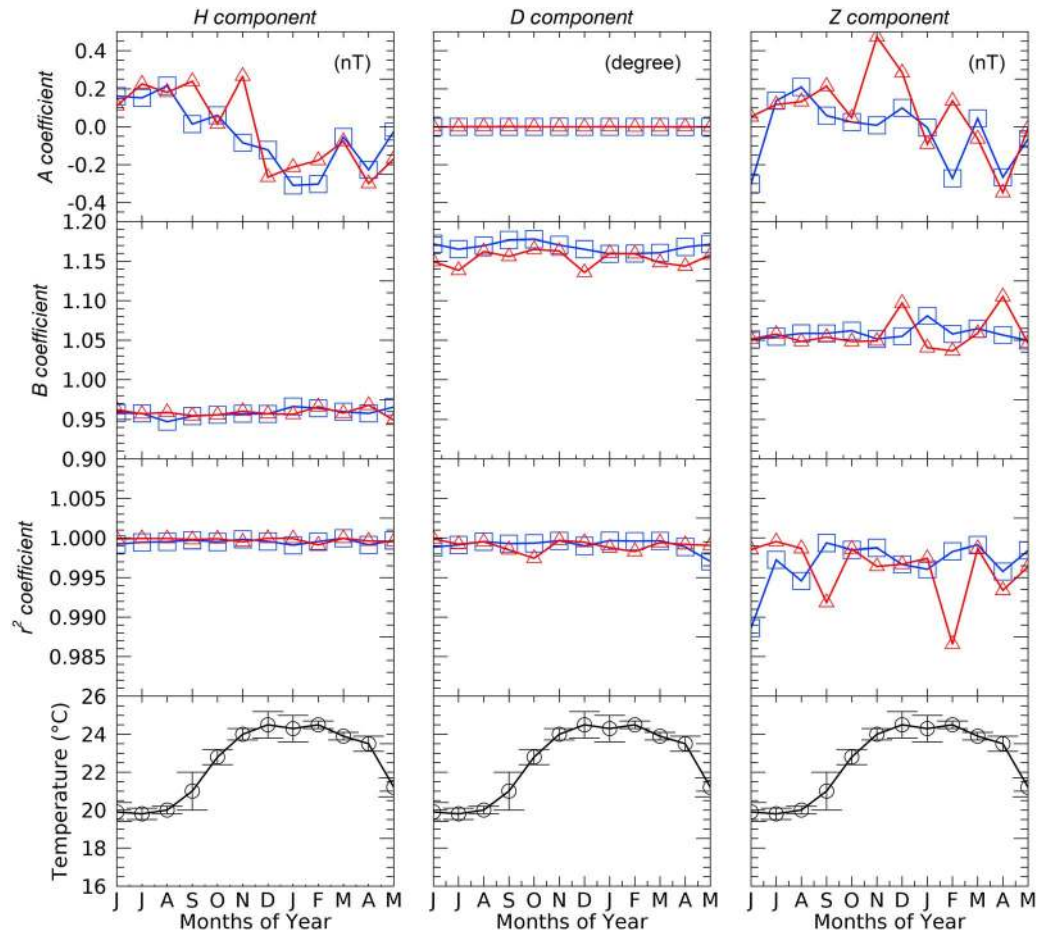
Figure 9. Variation of the monthly averaged linear (*A*), angular (*B*), and correlation (*r*^{2}) coefficients obtained from the linear fit between the Embrace and Intermagnet magnetic data collected from June 2015 until May 2016 in VSS, along with the monthly average temperature (*T*). The blue lines are for the quiet days, while the red lines are for the disturbed days.

magnetic field, in which excursion was picked up at around 50 nT (for the *H* component) at the VSS observatory. Consequently, errors of the order of 1–2% represent 0.5–1 nT. Therefore, these differences in the errors for the quiet and disturbed periods lie about the instrumental error. Thus, we assume that the mean error truly represents the gain matching error for each magnetic component individually, irrespective of the magnetic condition.

Thereafter, we checked the response of the gain matching error with the temperature (°C) variation. Figure 9 shows the variation monthly averaged coefficients obtained from the linear fit (which is a direct measurement of the error) between the Embrace and Intermagnet magnetic data collected from June 2015 until May 2016 in VSS. The linear (*A*) coefficients are plotted in the top panels, the angular (*B*) coefficients are in the panels of the second line, and the linear correlation (*r*^{2}) coefficient can be seen in the panels of the third line. The left panels of Figure 9 correspond to the analysis performed by the *H* magnetic components, the middle panels present the results for the *D* magnetic components, and the right panels show the results for the *Z* magnetic components. The blue lines with squares show the variation of the coefficients for the quiet days, while the red line with triangles show the variation of the coefficients for the disturbed days. The variation of the monthly average temperature measured at the sensor of the Embrace MagNet magnetometer is plotted as black line with circles in the bottom panels. Note that the sensor temperature of the magnetometer is repeated for the three magnetic components.

The temperature reached almost 25°C during the D months, while it remained around 20–22°C during the E and J months. In a general view, the values of the linear coefficients (*A*) for *H* and *Z* magnetic components

Table 6
The Linear (|A|), the Angular (B), and the Pearson Product Moment Correlation (r^2) Coefficients of the Linear Fit Between the Embrace MagNet and Intermagnet at the Vassouras Magnetic Observatory, Brazil

Period		H component			D component			Z component		
		|A| in nT	B	r^2	|A| in °	B	r^2	|A| in nT	B	r^2
J months	Qday	0.13385	0.99946	0.99948	0.00024	1.00736	0.99831	0.00375	0.99487	0.99483
	Dday	0.04884	1.00087	0.99979	0.00013	0.99224	0.99933	0.08196	0.99252	0.99830
D months	Qday	0.04467	0.99926	0.99957	0.00043	1.00831	0.99913	0.02175	1.00145	0.99820
	Dday	0.01330	1.00022	0.99972	0.00029	0.99323	0.99858	0.03863	1.00684	0.99565
E months	Qday	0.21289	1.00379	0.99950	0.00020	1.00234	0.99933	0.03517	1.00293	0.99741
	Dday	0.01504	1.00114	0.99961	0.00024	0.99431	0.99896	0.18358	0.99776	0.99437
Mean		0.07810	1.00079	0.99961	0.00010	0.99963	0.99894	0.03291	0.99939	0.99646

seem to have an anticorrelation dependence upon the temperature. However, they varied around ±0.5 nT, which is inside the instrumental error margin. The variation for the D magnetic components fluctuated in the third to fourth decimal place of 1°. Therefore, we cannot stare that the dependence on the temperature is real. The angular (B) and the correlation (r^2) coefficients do not present any dependence with the temperature at all. They practically remained constant along the whole period. Finally, the evolution of the coefficients does not show any appreciable dependence of the magnetic condition, as we can identify when comparing the red and blue lines in this figure.

Consequently, we can conclude that the variation of the temperature does not modify the correlation between the two different magnetometers (Embrace and Intermagnet). In other words, an eventual dependence with the temperature would affect both equipment in the same way, which agrees with the results from the previous analysis. Therefore, since the temperature does not cause any independent effect on the Embrace MagNet sensor measurements, it was not necessary to take it into account in our calibration procedure. Consequently, the average electronic gain errors found in this analysis were applied to each magnetic component of the entire set of magnetometers from the Embrace MagNet. Therefore, the measurements of this new magnetometer network now matches to the Intermagnet measurements.

Notwithstanding the effort to provide amplitude values comparable to an IAGA standard magnetometer through the Embrace MagNet sensor, the readers (users) shall be aware that that the offset of the fluxgate magnetometers are not constantly evaluated against the Intermagnet proton magnetometers. Therefore, the absolute values given by the Embrace MagNet may contain uncalibrated instrumental offset inherent in the fluxgate magnetometers. However, such eventual uncalibrated instrumental offset will be constant throughout the entire Embrace MagNet network of sensors due to the intercalibration process.

3.4. Embrace MagNet Data Quality Analysis Check

After applying the gain matching to all the magnetometer of the Embrace MagNet, we then proceeded with data quality analysis in order to verify if the gain matching succeeded properly. We performed another linear fit between H, D, and Z geomagnetic components acquired by the Embrace MagNet and Intermagnet networks during the same period used for the gain matching procedure. We are considering the five quietest and the five most disturbed days of each month. The data were classified from the first quietest (disturbed) day at 00h00 to the fifth quietest (disturbed) day at 23h59 UT with 1 min resolution. The linear (A) and angular (B) coefficients resulting from this new linear fit are shown per magnetic components in the columns of Table 6, along with the correlation (r^2) coefficient. They are averaged according to the disturbance level per season in the rows, and the overall averaged values are presented in the bottom line of this table. We expected that the linear coefficient (A) of the different magnetic components would tend to zero and that the angular coefficient (B) would tend to one in order that the relationship expressed in equations (1a), (1b), and (1c) demonstrate that the data collected by the Embrace MagNet would be equivalent to the same data collected by the Intermagnet network.

$$\Delta H_{VSSi}(t) \cong A_H + B_H \Delta H_{VSS}(t) \tag{1a}$$

$$\Delta D_{VSSi}(t) \cong A_D + B_D \Delta D_{VSS}(t) \tag{1b}$$

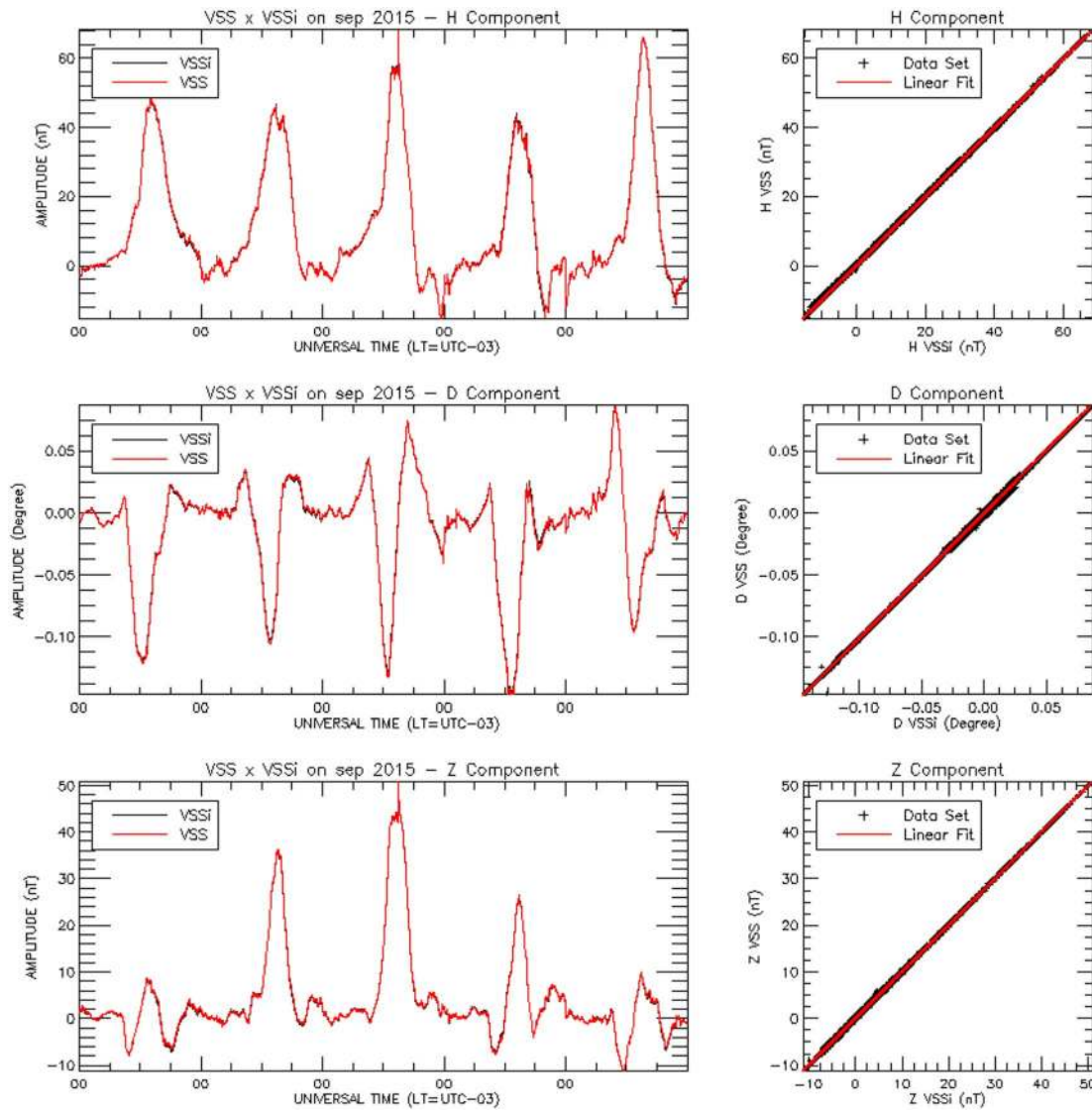$$\Delta Z_{VSSi}(t) \cong A_Z + B_Z \Delta Z_{VSS}(t) \tag{1c}$$

Figure 10. Diurnal variation (left panels) of the *H*, *D*, and *Z* magnetic component (from top to the bottom) measured on September 2015, at VSS, by the reference equipment (black line) and by the magnetometer under evaluation (red line), and the scatterplots (right panels) of the 5 most quietest days reference versus the 5 most quietest days under evaluation (black "+") for the same period, with the estimated linear fit curve (red line).

Indeed, the overall averaged values show that linear coefficients (offsets) are 0.07810 nT, 0.00010°, and 0.03291 nT for the *H*, *D*, and *Z* geomagnetic components, respectively. When we compared these "errors" with the maximum resolution specified in Table 4 for the Embrace MagNet, we noted that they lie below the resolution threshold. Thus, we can now assume they are negligible. In addition, the resulting overall averaged angular coefficients are 1.00079, 0.99963, and 0.99939 for the *H*, *D*, and *Z* geomagnetic components, respectively. Hence, they fall in the angular coefficients equals 1 with ±0.08% maximum error. Such "error" represents an uncertainty of 0.16 nT in the variation *H* geomagnetic component, assuming its maximum expected values measured at the dip equator (roughly 200 nT at midday). Again, as per the maximum resolution specified in Table 4 for the Embrace MagNet, such uncertainty lies below the resolution threshold. Consequently, we can state that the angular coefficients are equal to the unit. In support of these statements, all the three correlation coefficients resulted to higher than 99.6%, which shows that the data collected by the Embrace MagNet is highly correlated with those data collected by the Intermagnet network.

With respect to the differences in the *H*, *D*, and *Z* geomagnetic components measured by the Embrace MagNet in contrast with the same measurement made with the Intermagnet sensor considering the
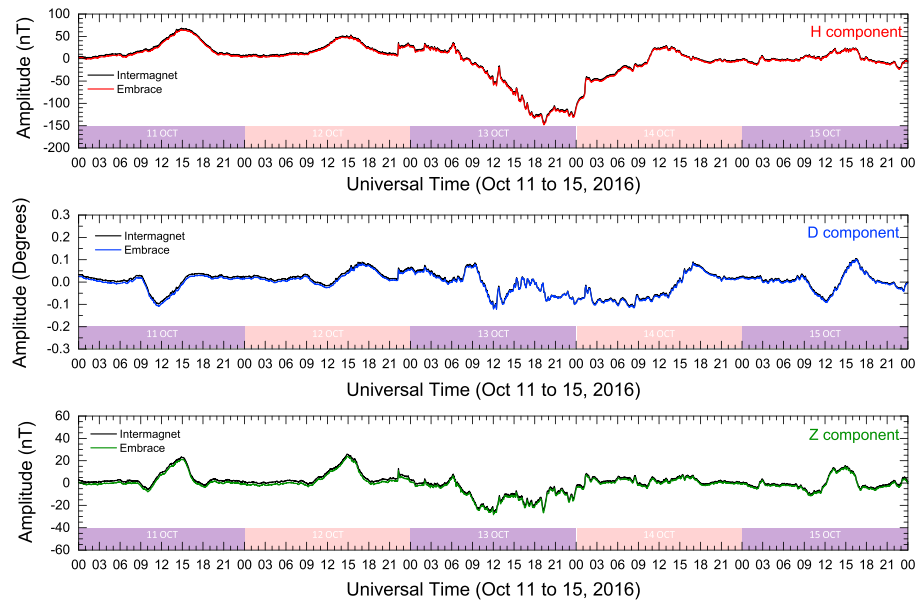
Figure 11. Diurnal variation of the (top) *H*, (middle) *D*, and (bottom) *Z* magnetic component measured from 11 to 15 October 2016, at VSS, by the reference equipment (black line) and by the Embrace magnetometer (colored lines).

magnetic conditions (quiet and disturbed), we only noted differences in the linear coefficients for the analysis of the *H* and *Z* components. The difference lies close to the resolution threshold specified in Table 1, whereas no difference is noted between the magnetically quiet and disturbed periods for the angular coefficients and the correlation coefficients obtained for all the geomagnetic components. Thereby, the results show that the magnetic conditions equally affect the data collected by both networks.

Moreover, the correlation analysis investigated in terms of the season reveals that no appreciable difference can be noted when comparing the averaged coefficient calculated for J, D, and E months for the *H*, *D*, and *Z* components. Taking, for instance, the angular coefficient for equation (1a), we see it varying from 0.99926 to 1.00379. This represents a maximum excursion of 0.5% inside the year, which we consider acceptable for the studies of ionospheric currents. Thus, in our view, the seasonal variations cause no effect on the correlation values between the data collected by both networks.

As a partial conclusion on this subject, we consider that the data collected by Embrace MagNet during quiet time are equivalent to those collected by the Intermagnet network at the same site, irrespective of the geomagnetic conditions and season. To support this conclusion, we present the Figure 10 with an example of the daily variation of the magnetic components (*H* in the top graphs, *D* in the middle graphs, and *Z* in the bottom graphs) at VSS after the gain matching process to be completed. The figure shows the five quietest days in September 2015 (left panel) of the Embrace MagNet and Intermagnet and their correlation (right panels). The black line in the figure shows the Intermagnet magnetometer used as reference equipment (identified as VSSi) and the red line the magnetometer belonging to the Embrace MagNet that was under evaluation (identified as VSS). In addition, we present the scatterplots (black "+") of the reference Intermagnet observatory data versus Embrace data under evaluation in the right panel, with the estimated linear fit curve (red line).

All the amplitudes of the magnetic components measured by both magnetometers, as well as its temporal response, are in a good match, as shown in Figure 10. In addition, the almost perfect alignment of the dots in the right panel added to the high-correlation factor that reinforces such good relationship between the Embrace magnetometer measurements in relation to the measurements of the reference Intermagnet magnetometer. Irrespective of this good result, one of our goals is to use the Embrace MagNet for providing reliable data during disturbed magnetic conditions. Therefore, we also checked the behavior of both sensors (Embrace and Intermagnet) during storm time, but using data collected in a period outside the period of analysis. Consequently, we present Figure 11 with an example of the daily variation of the magnetic components

(*H*, *D*, *Z*) at VSS after the gain matching process to be completed. The figure shows the five consecutive days from 11 to 15 October 2016 (during an intense magnetic storm). The black line in the figure shows the absolute magnetometer used as reference equipment (Intermagnet) and the colored lines the magnetometer belonging to the Embrace MagNet that was under evaluation. The components are identified in the top right corner in each graph.

To this point and after observing the result shown in Figure 11, we are confident to state that all the amplitudes of magnetic components measured by both magnetometers during any magnetic condition, as well as its spectral and temporal response, are in a good match with an absolute standard magnetometer. Finally, as a general conclusion on this subject, we now consider that the data collected by Embrace MagNet are equivalent to those collected by the Intermagnet network at the same site, irrespective of the geomagnetic conditions and season.

4. Concluding Remarks

A new fluxgate magnetometer network has risen to fulfill a gap for magnetic measurement available online in South America. We have briefly described the magnetometer used to monitor the geomagnetic field. We have described the network and the procedure used to calibrate the entire network sensors. In addition, we presented the averaged square error for each individual magnetic component and for the total field, which resulted to be of the order of the equipment resolution. Proper care with the intercalibration of the whole network was applied to assure the consistency of the measurement made at each single magnetic station. Therefore, we assure the consistency of the network as a unit. Subsequently, we performed a study using the data collected at the Vassouras Magnetic Observatory, covering the period from June 2015 to May 2016. In such study, we validated the magnetic data of the Embrace MagNet using a correlation with the Intermagnet data.

Our results show that the Embrace MagNet data had a constant error in the amplitude of the magnetic components, irrespective of the temperature, magnetic condition, and season of the year. Based on that, we correct the gain of the Embrace MagNet sensors. The *H* component values were increased by 4.2%, whereas the *D* values were decreased by 16.1% and the *Z* component was decreased by 5.8%. After applying such gains to our data, we guarantee that the network provides magnetic measurements very close to the absolute measurements. Consequently, we develop a network of magnetometer stations that is able to provide results that are comparable to the absolute measurement made at magnetic observatories, which are suitable for space weather studies. Afterward, we presented a companying paper (Denardini et al., 2018) where the reader can find a series of scientific findings along with recent publication based on the data collected by the Embrace MagNet to support that.

Finally, we would like to remark that several stations are fully operational, and we have shown samples of the capability of this new magnetic network. It is equally important to mention that its main goal is to provide data with quality suitable enough for space weather studies, including creating the South American *K* index (*Ksa*). Furthermore, the collected data are fully open and accessible in acknowledgment basis at the Embrace Program website (http://www.inpe.br/spaceweather).

References

Chapman, S., & Bartels, J. (1940). *Geomagnetism* (Vol. 2). London: Oxford University Press.

Denardini, C. M., Abdu, M. A., Aveiro, H. C., Resende, L. C. A., Almeida, P. D. S. C., Olívio, Ê. P. A., et al. (2009). Counter electrojet features in the Brazilian sector: Simultaneous observation by radar, digital sounder and magnetometers. *Annales Geophysicae*, 27(4), 1593–1603. https://doi.org/10.5194/angeo-27-1593-2009

Denardini, C. M., Chen, S. S., Resende, L. C. A., Moro, J., Bilibio, A. V., Fagundes, P. R., et al. (2018). The embrace magnetometer network for South America: First scientific results. *Radio Science*, 53. https://doi.org/10.1002/2018RS006540

Denardini, C. M., Dasso, S., & Gonzalez-Esparza, J. A. (2016a). Review on space weather in Latin America. 2. The research networks ready for space weather. *Advances in Space Research*, 58(10), 1940–1959. https://doi.org/10.1016/j.asr.2016.03.013

Denardini, C. M., Dasso, S., & Gonzalez-Esparza, J. A. (2016b). Review on space weather in Latin America. 3. Development of space weather forecasting centers. *Advances in Space Research*, 58(10), 1960–1967. https://doi.org/10.1016/j.asr.2016.03.011

Denardini, C. M., Rockenbach, M., Gende, M. A., Chen, S. S., Fagundes, P. R., Schuch, N. J., et al. (2015). The initial steps for developing the South American *K* index from the Embrace Magnetometer Network. *Brazilian Journal of Geophysics*, 33(1), 79–88.

Gonzalez, W. D., Joselyn, J. A., Kamide, Y., Kroehl, H. W., Rostoker, G., Tsurutani, B. T., & Vasyliunas, V. M. (1994). What is a geomagnetic storm? *Journal of Geophysical Research*, 99(A4), 5771–5792. https://doi.org/10.1029/93JA02867

Jankowski, J., & Sucksdorff, C. (1996). *Guide for magnetic measurements and observatory practice* (p. 232). Boulder: IAGA.

Lindzen, R. S., & Chapman, S. (1969). Atmospheric tides. *Space Science Reviews*, 10(1), 3–188. https://doi.org/10.1007/BF00171584

Maeda, K., & Kato, S. (1966). Electrodynamics of the ionosphere. *Space Science Reviews*, 5(1), 57–79. https://doi.org/10.1007/BF00179215

Matsushita, S. (1969). Dynamo currents, winds and electric fields. *Radio Science*, 4(9), 771–780. https://doi.org/10.1029/RS004i009p00771

Moro, J., Denardini, C. M., Correia, E., Abdu, M. A., Schuch, N. J., & Makita, K. (2012). Correlation between the cosmic noise absorption calculated from the SARINET data and the energetic particles measured by MEPED: Simultaneous observations over SAMA region. *Advances in Space Research*, 51, 1692–1700.

Ripka, P. (1992). Review of fluxgate sensors. *Sensors and Actuators A*, 33(3), 129–141. https://doi.org/10.1016/0924-4247(92)80159-Z

Schrijver, C. J., Kauristie, K., Aylward, A. D., Denardini, C. M., Gibson, S. E., Glover, A., et al. (2015). Understanding space weather to shield society: A global road map for 2015–2025 commissioned by COSPAR and ILWS. *Advances in Space Research*, 55(12), 2745–2807. https://doi.org/10.1016/j.asr.2015.03.023

Schulte in den Bäumen, H., Moran, D., Lenzen, M., Cairns, I., & Steenge, A. (2014). How severe space weather can disrupt global supply chains. *Natural Hazards and Earth System Sciences*, 14(10), 2749–2759. https://doi.org/10.5194/nhess-14-2749-2014

Trivedi, N. B., Vitorello, I., Kabata, W., Dutra, S. L. G., Padilha, A. L., Bologna, M. S., et al. (2007). Geomagnetically induced currents in an electric power transmission system at low latitudes in Brazil: A case study. *Space Weather*, 5, S04004. https://doi.org/10.1029/2006SW000282

Veliz, O. (2010). *Manual de Operación: JRO-ML-103 triaxial magnetometer*. Lima, Peru: Jicamarca Radio Observatory.

Vestine, E. H. (1960). The upper atmosphere and geomagnetism. In J. A. Ratcliffe (Ed.), *Physics of the upper atmosphere* (Chap. 10, pp. 471–512). New York: Academic Press.